JOURNAL OF SYNCHROTRON RADIATION

ISSN 1600-5775

Utilizing broadband X-rays in a Bragg coherent X-ray diffraction imaging experiment

Wonsuk Cha,[a] Wenjun Liu,[b] Ross Harder,[b] Ruqing Xu,[b] Paul H. Fuoss[a] and Stephan O. Hruszkewycz[a]*

[a]Materials Science Division, Argonne National Laboratory, Argonne, IL 60439, USA, and [b]X-ray Science Division, Argonne National Laboratory, Argonne, IL 60439, USA. *Correspondence e-mail: shrus@anl.gov

Received 11 January 2016
Accepted 28 June 2016

Edited by G. E. Ice, Oak Ridge National Laboratory, USA

Keywords: coherent X-ray diffraction imaging; polychromatic X-ray diffraction; materials characterization.

A method is presented to simplify Bragg coherent X-ray diffraction imaging studies of complex heterogeneous crystalline materials with a two-stage screening/imaging process that utilizes polychromatic and monochromatic coherent X-rays and is compatible with *in situ* sample environments. Coherent white-beam diffraction is used to identify an individual crystal particle or grain that displays desired properties within a larger population. A three-dimensional reciprocal-space map suitable for diffraction imaging is then measured for the Bragg peak of interest using a monochromatic beam energy scan that requires no sample motion, thus simplifying *in situ* chamber design. This approach was demonstrated with Au nanoparticles and will enable, for example, individual grains in a polycrystalline material of specific orientation to be selected, then imaged in three dimensions while under load.

1. Introduction

The performance of modern materials across a broad spectrum of applications relies on properties, interactions and heterogeneity at nanometer to micrometer length scales. Thus, characterizing the local structure in materials at these length scales under realistic conditions is critical for optimizing performance. Bragg coherent diffraction imaging (BCDI) shows great potential in this area, and has recently been used to nondestructively image the internal strain in nanoscale crystals under *in situ* conditions (Cha *et al.*, 2013; Ulvestad *et al.*, 2015; Clark *et al.*, 2015). However, as currently implemented, BCDI utilizes a single-wavelength monochromatic X-ray beam. As a result, the sample must be rotated in order to measure a data set that yields a three-dimensional (3D) image, limiting the design of *in situ* experiments. Furthermore, a monochromatic beam accesses a limited volume of reciprocal space, such that the behavior of multiple particles in an ensemble is difficult to simultaneously survey, for example, to identify a single grain in a volume that responds most strongly to an applied impulse.

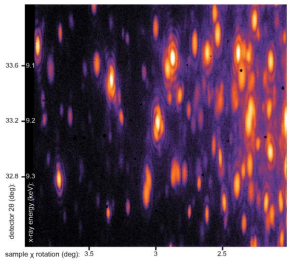

Here, we address both of these challenges by introducing a two-stage approach to BCDI that utilizes the broadband coherent X-ray spectrum of a third-generation synchrotron source. We demonstrate that a coherent white beam can be used to survey a broad swath of reciprocal space in order to identify individual crystallites of interest. Upon identifying a crystalline grain or particle for study, a monochromator is translated into the beam and used to measure a volume of reciprocal space by scanning energy (Cornelius *et al.*, 2011), thus allowing the sample to remain stationary while obtaining data needed for 3D imaging. Such a two-stage screening/

imaging capability can be a powerful way to study individual crystallites in an ensemble when the exact orientation and location of the most responsive subset of crystals is not known *a priori* (Lind *et al.*, 2014; Ice *et al.*, 2011). We demonstrated this concept by identifying an individual gold nanoparticle from a population of textured orientations using white-beam coherent diffraction, then measuring its 3D Bragg coherent diffraction pattern with a monochromatic beam energy scan without moving the sample.

2. Experiment

The measurement was performed at the Sector 34-ID-E beamline at the Advanced Photon Source. This beamline is equipped with a double-crystal monochromator that can be translated into and out of the incoming X-ray beam, thus allowing collimated monochromatic or polychromatic (white beam) X-rays to illuminate the same area of the sample (see Fig. 1) (Ice *et al.*, 2000). The Si (111) monochromator was positioned 5 m upstream of the sample and is capable of scanning energy in increments as small as 1 eV. The incoming X-ray source size was defined in the horizontal direction by slits 30 m upstream of the sample (0.1 mm wide) and in the vertical direction by the size of the beam from the undulator (30 µm), 60 m from the sample. With such a source size, the horizontal (H) and vertical (V) transverse coherence lengths (without focusing) were determined to be 65 µm and 35 µm, respectively, *via* fringe visibility measurements from grating scattering. The size of the beam at the sample was determined by secondary slits set to 50 µm (H) × 100 µm (V) positioned 0.85 m from the sample. The energy spectrum of the undulator used in this study is shown in Fig. 2, set to peak at 9.21 keV with ∼250 eV FWHM (no taper).

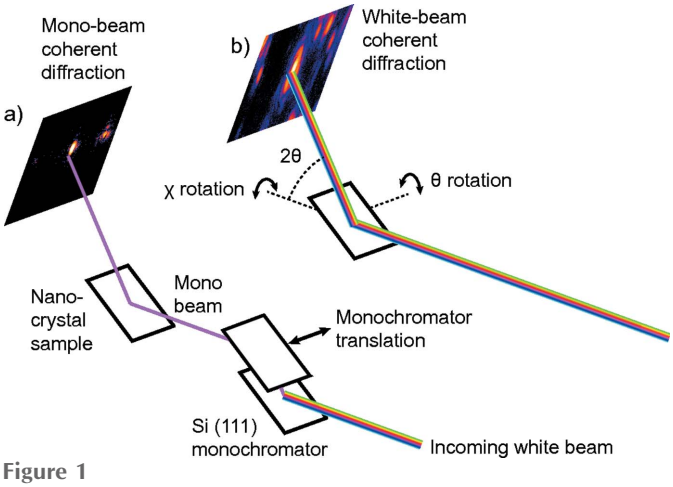

Figure 1
Schematic of a coherent diffraction beamline equipped with a monochromator that can be translated into and out of the white beam. (*a*) With the monochromator in the white beam, a coherent monochromatic beam is delivered to the sample, and a typical coherent diffraction pattern is measured when a nanocrystalline sample and area detector are positioned to satisfy a Bragg condition. (*b*) With the monochromator positioned out of the beam, a white-beam coherent diffraction pattern can be measured that surveys the orientation and size of multiple crystals illuminated with the beam.

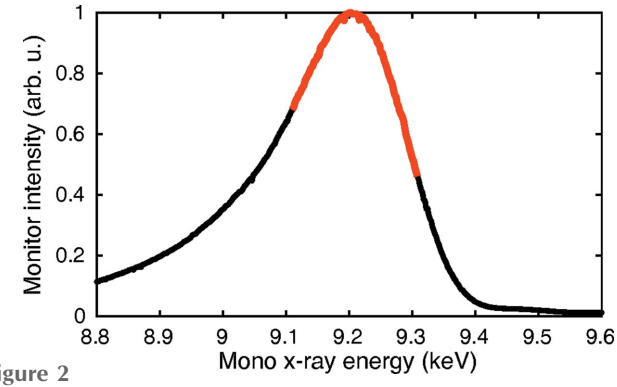

Figure 2
The undulator spectrum used in the coherent white-beam measurement in this work. The experimental geometry was such that the peak of the undulator spectrum (9.21 keV) was diffracted into the central 2θ pixel of the detector (as shown in Fig. 2) when scattering from Au (111) planes. The red portion of the curve indicates the energy range over which a monochromator energy scan was performed to measure the 3D coherent fringes of the Bragg peak of interest.

A sample consisting of Au nanoparticles on a [001]-surface-normal-oriented Si substrate was used in this study. The Au nanoparticles were approximately spherical, ∼200–400 nm in diameter. They were oriented such that $[111]_{Au}||[001]_{Si}$, with a textured distribution of orientations (∼0.4° FWHM). The vertical diffraction geometry (Fig. 1) was such that the 111 Au Bragg condition was satisfied at an X-ray energy of 9.21 keV. Thus, the angle of the sample relative to the incident beam (θ) was set to 16.2° and the center of the area detector (Pixirad-1 with CdTe sensor) was positioned at a 2θ angle of 33.2°. The sample-to-detector distance was 860 mm, and the detector had hexagonal pixels of width 60 µm.

3. Results and discussion

Fig. 3 shows a measured coherent diffraction pattern containing 111 Bragg peaks from multiple Au particles illuminated with an unfocused white beam (spectrum shown in Fig. 2). The pattern was measured with the sample tilted in χ by 0.3° from the surface normal of the substrate, near the tail of the textured particle orientation distribution. Because of this tilting in χ, the number of Au Bragg peaks in the detector increases from left to right, towards the peak of the orientation distribution near $\chi = 0°$. In the 2θ detector dimension, Au Bragg peaks are visible from particles with different orientations along θ. [Particles with different lattice parameters would also appear at different 2θ values, but here the Au crystals were determined to have a uniform (111) lattice spacing.] Multiple crystals with different orientations along θ are visible because of the broad bandwidth of the incoming white beam. Particles with Bragg peaks in the bottom half of the detector (lower 2θ) diffract higher-energy photons from the spectrum, and high 2θ peaks consist of lower-energy photons. Particles that diffract into the central 2θ range of the detector diffract photons near the peak of the undulator spectrum at 9.21 keV.

We note that coherent diffraction fringes are seen decorating the Bragg peaks from individual Au nanoparticles

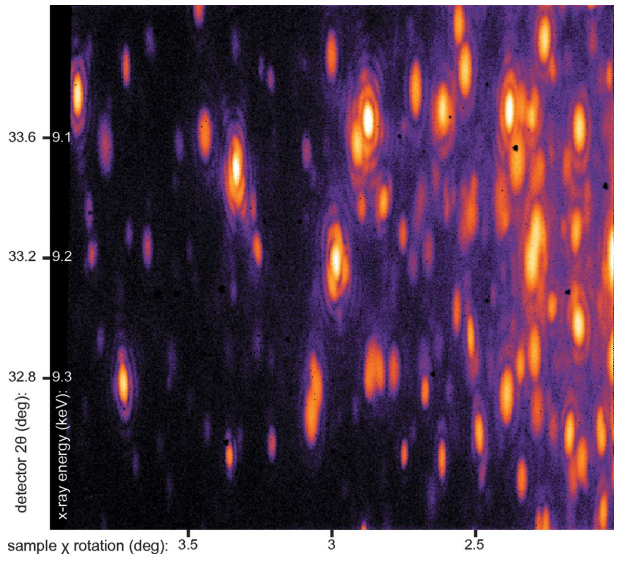

Figure 3
A coherent white-beam diffraction pattern featuring Au 111 Bragg peaks from a collection of nanoparticles with slightly different orientations. This image shows that the majority of Au particles scattering into the detector are oriented to diffract to the right-hand side, nearer to the surface-normal of the Si substrate. Using such a survey map, one can identify individual particles are both well separated in reciprocal space from other scattering particles and have a desired orientation with respect to the ensemble average particle orientation.

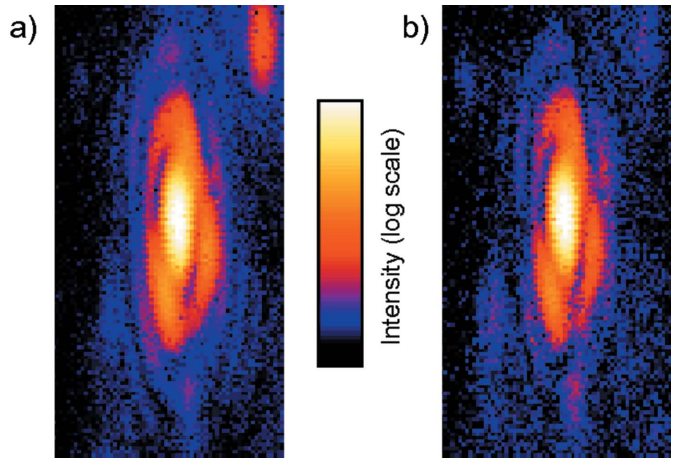

Figure 4
Comparison of the central Bragg peak in the detector measured with (*a*) a white beam, with (*b*) a summation of 100 individual monochromatic diffraction patterns collected in 2 eV energy steps over the energy range indicated in red in Fig. 2.

due to the high degree of transverse coherence of the white beam. These fringes are a projection of the 3D coherent Bragg diffraction pattern onto the detector plane over a range of incident beam energies [a concept explored in simulation by Ice *et al.* (2009)]. This was confirmed by translating the monochromator into the beam and performing an energy scan over the range indicated in red in Fig. 2 with 2 eV steps. Fig. 4 shows the white-beam Bragg diffraction pattern in the center of the detector (*a*) compared with a summed image of the monochromatic beam energy scan (*b*), and the two are very similar. Small differences arise due to slight differences in the position of the monochromatic and white beams. Differences in the longitudinal coherence of the diffracted X-ray beam likely contributes to small differences in the expected fringe visibility of the two patterns, but the fringe visibility of the two patterns shown here are indistinguishable within noise.

The primary utility of the coherent monochromatic beam energy scan is to enable the fringes of this Bragg peak to be resolved in three dimensions. As shown in Fig. 5(*a*), changing the wavelength λ of the incoming X-rays changes the length of the reciprocal-space scattering vector $q = k_f - k_i$ (where $|k_i| = |k_f| = 2\pi/\lambda$). By stepping energy in sufficiently fine increments (Cornelius *et al.*, 2011), the volume of reciprocal surrounding a Bragg peak can be measured [gray parallelogram in Fig. 5(*a*)]. In order to represent the 3D scattering information measured in this experiment, we calculated the value of q corresponding to the center of each hexagonal pixel in the detector at each

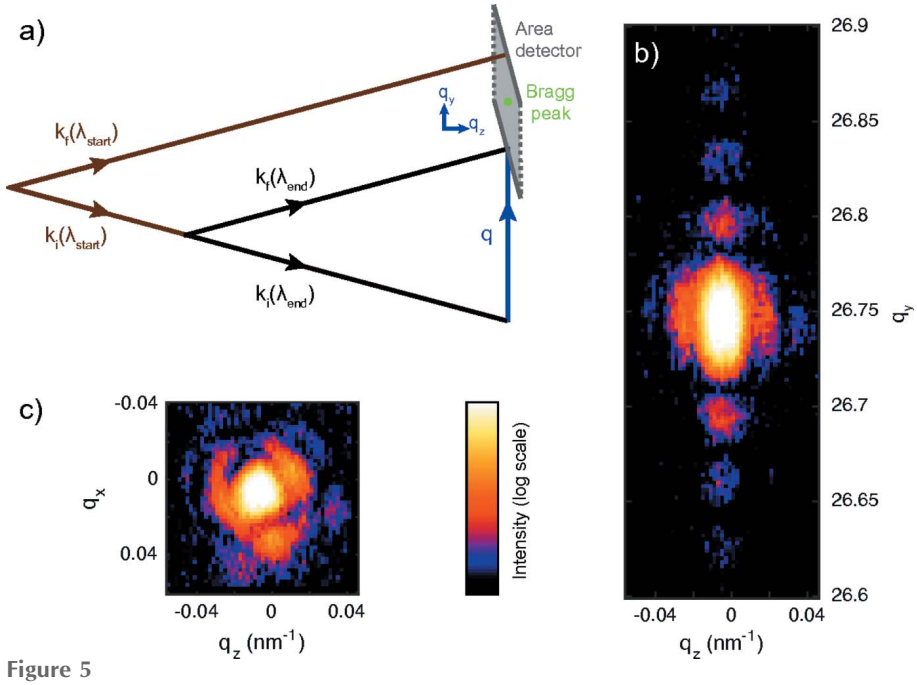

Figure 5
The geometry of a monochromatic beam energy scan is shown in (*a*). Changing energy from low (λ_{start}) to high (λ_{end}) changes the length of the reciprocal-space vector q. In this experiment, the Au Bragg peak in the center of the detector in Fig. 3 was scanned with a monochromator in 2 eV energy steps such that a volume of reciprocal space [gray parallelogram in (*a*)] was finely sampled. The resulting diffraction was interpolated onto a regular reciprocal-space grid, and two cuts are shown along the (q_z, q_y) plane (*b*) as well as the (q_z, q_x) plane (*c*) through the center of the Bragg peak.

energy step. Using these q-space coordinates, the recorded intensity was interpolated onto a regular q-space grid, along the principle axes q_x, q_y, q_z indicated in Fig. 5(a). Two interpolated orthogonal cuts through the reciprocal-space volume surrounding the Au 111 Bragg peak are shown in Figs. 5(b) and 5(c). These cuts show the characteristic fringes associated with a gold nanoparticle, indicating a faceted flattened circular shape approximately 360 nm in diameter and 150 nm in height. Such a 3D coherent diffraction pattern with well defined fringes is well suited for 3D imaging with BCDI, and can be measured without changing the position of the sample.

We also note that the time resolution of the 3D Bragg peak measurement can potentially be improved by replacing the monochromatic beam energy scan with a system of multi-angle semi-transparent analyzer crystals acting to disperse the Bragg-diffracted white beam in energy and angle. This concept is presented in Fig. 6 and is based on introducing a series of thin X-ray-transparent single-crystal membrane analyzer crystals into the diffracted white beam from the sample. The analyzers are positioned at slightly different angles relative to the white-beam Bragg peak such that each analyzer diffracts photons of unique energy and exit angle into an area detector. With an appropriate transform, the measured intensity pattern can then be translated to regular q_x, q_y, q_z coordinates, as in Fig. 5. If realised, such a capability would enable 3D reciprocal-space maps suitable for BCDI to be collected with a small number of rapid white-beam exposures to the sample. The gains in time resolution would scale with the number of transparent analyzers introduced in the diffracted beam. For example, if five analyzer membranes are introduced separated by small angles ($\sim$0.1°), then five 'cuts' about the Bragg peak can be accessed at once. Thus, in this case, one-fifth of the number of exposures are theoretically needed in an analyzer angle scan ($\theta_{\rm ana}$) as compared with a monochromatic beam sample angle scan ($\theta_{\rm sam}$). Preliminary experiments performed with 2 µm-thick Si crystal membranes suggest that such a five-analyzer arrangement may be feasible, and the concept can conceivably be extended to incorporate more analyzers.

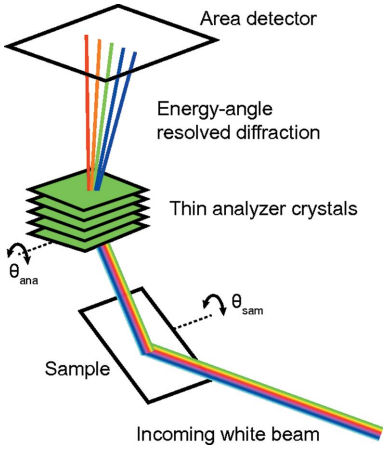

Figure 6
Schematic outlining the concept of white-beam diffraction analyzers for resolving the energy/angle components of the beam diffracting from the sample. This concept is based on introducing a series of thin X-ray transparent single-crystal membrane analyzer crystals into the diffracted white beam from the sample.

The capability outlined here (*i.e.* utilizing a coherent white beam to survey a population of differently aligned crystallites, identifying one for 3D imaging, and employing a fixed-sample-position energy scan with a monochromatic beam) potentially increases the scope of *in situ* 3D imaging studies feasible with BCDI. Firstly, in systems with complex heterogeneous local structure, it is often difficult to predict which local volumes will respond to a given environmental change (*i.e.* applied stress, voltage, chemical environment). Thus simultaneously screening a larger population of particles with a white beam is advantageous for quickly identifying a maximally responsive crystal or grain for 3D BCDI imaging. Secondly, by utilizing an energy scan to record the 3D volume surrounding the Bragg peak of the selected crystallite (as compared with a sample angle scan), the sample itself remains stationary during the measurement. This allows for greater latitude in designing complex environmental chambers for *in situ* studies where sample motion is cumbersome (Cornelius *et al.*, 2012).

Acknowledgements

This work, including use of the Advanced Photon Source, was supported by the US Department of Energy, Office of Science, Office of Basic Energy Sciences, under Contract No. DE-AC02-06CH11357. PHF and SOH were supported by US DOE, Basic Energy Sciences, Materials Sciences and Engineering Division.

References

Cha, W., Jeong, N. C., Song, S., Park, H., Thanh Pham, T. C., Harder, R., Lim, B., Xiong, G., Ahn, D., McNulty, I., Kim, J., Yoon, K. B., Robinson, I. K. & Kim, H. (2013). *Nat. Mater.* **12**, 729–734.
Clark, J. N., Ihli, J., Schenk, A. S., Kim, Y.-Y., Kulak, A. N., Campbell, J. M., Nisbet, G., Meldrum, F. C. & Robinson, I. K. (2015). *Nat. Mater.* **14**, 780–784.
Cornelius, T. W., Carbone, D., Jacques, V. L. R., Schülli, T. U. & Metzger, T. H. (2011). *J. Synchrotron Rad.* **18**, 413–417.
Cornelius, T. W., Davydok, A., Jacques, V. L. R., Grifone, R., Schülli, T., Richard, M.-I., Beutier, G., Verdier, M., Metzger, T. H., Pietsch, U. & Thomas, O. (2012). *J. Synchrotron Rad.* **19**, 688–694.
Ice, G. E., Budai, J. D. & Pang, J. W. L. (2011). *Science*, **334**, 1234–1239.
Ice, G. E., Chung, J.-S., Lowe, W., Williams, E. & Edelman, J. (2000). *Rev. Sci. Instrum.* **71**, 2001–2006.
Ice, G. E., Pang, J. W. L., Larson, B. C., Budai, J. D. Z. T. J., Tischler, J. Z., Choi, J., Liu, W., Liu, C., Assoufid, L., Shu, D. & Khounsary, A. (2009). *Mater. Sci. Eng. A*, **524**, 3–9.
Lind, J., Li, S. F., Pokharel, R., Lienert, U., Rollett, A. D. & Suter, R. M. (2014). *Acta Mater.* **76**, 213–220.
Ulvestad, A., Singer, A., Clark, J. N., Cho, H. M., Kim, J. W., Harder, R., Maser, J., Meng, Y. S. & Shpyrko, O. G. (2015). *Science*, **348**, 1344–1347.